AUTOMATIC IDENTIFICATION OF LUNG ABNORMALITIES IN CHEST SPIRAL CT SCANS

Ayman El-Baz1, Aly A. Farag,[1] Ph.D., Robert Falk, M.D.[2] and Renato La Rocca, M.D.[3]

[1] Computer Vision and Image Processing Laboratory, University of Louisville, Louisville, KY 40292
E-mail: {elbaz,farag}@cvip.Louisville.edu,URL: www.cvip.louisville.edu

[2] Director, Medical Imaging Division Jewish Hospital, , E-mail: robert.falk@jhhs.org

[3] Director, Kentuckiana Cancer Institute, E-mail: rvl@kci.us

ABSTRACT

This research aims at developing a fully automatic Computer-Assisted Diagnosis (CAD) system for lung cancer screening using chest spiral CT scans. One thousand subjects are enrolled in a chest cancer screening program in Louisville, KY, USA, which aims at quantification of the effectiveness of low dose spiral CT scans for early diagnosis of lung cancer, and evaluating its possible impact on improving the mortality rate of cancer patients. This paper presents an image analysis system for 3-D reconstruction of the lungs and trachea, detection of the lung abnormalities, identification/classification of these abnormalities with respect to specific diagnosis, and distributed visualization of the results over computer networks. We present two novel approaches for segmentation of the lung tissues from the surrounding structures in the chest cavity, and detection of the abnormalities in the lungs. The segmentation algorithm is hierarchical; it starts with isolating the background from the chest cavity, then isolating the lungs from the surrounding structures (e.g., ribs, liver, and other organs that may appear in chest CT scans). Abnormalities in the lungs are detected by analyzing the segmented lung tissues and extracting the isolated lumps that appear in various connected regions. 3-D reconstructions are also generated for these abnormalities, in order to be used for subsequent identification/classification steps. Results of these algorithms are shown on 50 subjects, and have been evaluated vs. the radiologists. The image analysis approach presented in this paper has provided comparable results with respect to the experts. The approach is quite fast, and lends itself to distributed visualization over computer networks.

1. INTRODUCTION

Lung Cancer remains the leading cause of mortality cancer. In 1999, there were approximately 170,000 new cases of lung cancer [1]. The 5-year survival rate from the diseases is 14% and has increased only slightly since the early 1970s despite an extensive and costly research effort to find effective therapy. The disparity in survival between early- and late-stage lung cancer is substantial, with a 5-year survival rate of approximately 70% in stage 1A disease compared to less than 5% in stage IV disease according to the recently revised Lung Cancer Staging criteria [1]. The disproportionately high prevalence and mortality of lung cancer has encouraged attempts to detect early lung cancer with screening programs aimed at smokers. Smokers have an incidence rate of lung cancer that is 10 times that of nonsmokers and account for greater than 80% of lung cancer cases in the United States [1]. In the recent years, a wealth of new technologies has emerged that are capable of detecting lung cancer at an early stage. These technologies include low-dose spiral CT (LDCT). LDCT has been explored as a tool for detecting early lung cancer in symptomatic individuals at a risk for this disease, with encouraging preliminary results [1]. LDCT can provide high spatial and high temporal resolution, excellent contrast resolution for the pulmonary structures and surrounding anatomy, and the ability to gather a complete three-dimensional (3-D) volume of the human thorax in a single breath hold [2].

The jewish hospital cancer screening and early detection study is a randomized trial with the following specific aims:

1. Determine whether the use of spiral ct scanning of the chest detects early lung abnormalities that lead to cancer, which are not visible on chest x-rays in patients at high-risk for developing lung cancer; and
2. Determine whether annual spiral chest ct scans of the chest in high-risk patients result in an improvement in survival
3. high-risk patients result in an improvement in survival

The Jewish Hospital document [3] details the approach followed in the ongoing Chest Cancer Screening Program. The document also states that the reasons behind the use of the dual modality approach (X-ray and CT) in the screening programs. The primary purpose of this screening study is to determine whether there is sufficient evidence to warrant routine screen for lung cancer via CT scanning. Patients will be sequentially accrued into the study. Using a randomized block design, patients will be placed in a chest x-ray only group or CT scanning group. The data will be reviewed yearly and the study will be stopped if sufficient evidence exists to conclude that survival is greater in the CT scanned group with p-value of less than 0.05. Once 1000 patients have been accrued, the data will again be analyzed for the next five years. Again, the study will be stopped if there is sufficient evidence to conclude that survival is greater in the CT-scanned group with a p-value of less than 0.05. At the end of five years, the full cohort will be studied to determine whether sufficient evidence exists or if additional patients need to be accrued [4]. Other screening chest cancer studies in the US include ELCAP [4] and ACRIN [5]. The Jewish Hospital screening program lends itself more into classification of calcified and non-calcified abnormalities in the Kentucky area by the Ohio Valley.

A number of groups have developed techniques for computer-assisted segmentation of pulmonary CT images (e.g., [6]-[9]). In [6], manually traced boundaries were used to estimate regional

gas and tissue volumes in the lungs of normal subjects. On two-dimensional (2-D) transverse slices of a pulmonary CT dataset, the natural contrast between the low-density lungs and surrounding high-density chest wall can be used to guide image segmentation. In [6][9] 2-D edge tracking was used to find the boundaries of the left and right lungs. The disadvantage of this algorithm is that errors can occur in detecting the edges; this error increases as the contrast of the CT decrease.

In this paper, we describe a fully automatic method for identification and visualization of the lungs and trachea for isolating blatant abnormalities in the lung, which spread over several slices in the spiral CT scans.

2. METHODS

2.1 DATA ACQUISITION

In Jewish hospital project, 1000 symptomatic patients greater than 60 years of age with positive smoking history (> 10 pack-years) will undergo screening with LDCT and chest radiography. The LDCT was performed with the following parameters: Slice thickness of 8 mm reconstructed every 4 mm, Scanning pitch 1.5. Our method consists of four main steps: 1) lung extraction; 2) abnormality detection; 3) identification/classification; and visualization.

2.2 LUNG EXTRACTION

The goal of the lung extraction step is to separate the voxels corresponding to lung tissue from those belonging to the surrounding anatomical structures. Since the gray level of the background is close to the gray level of the lung tissues, it is advantageous to remove the background (all pixels outside the chest cavity) from each slice before doing extraction of the lung regions, in order to increase the accuracy of segmentation. Background is simply removed as follows: starting from the edges of the CT slices, all pixels that have similar gray levels, within a certain range, are removed. This process is applied, on each slice, from the left to right corners (i.e., horizontally or row-wise) as well as vertically (column-wise), in order to cover the whole slice. This simple approach has been shown to be quite adequate for removal of the background pixels outside the chest cavity region.

After removing the background from each slice, we assume that each CT slice (image) contains only two types of pixel: 1) Lungs - pixels within very dense regions in the CT scan. These pixels have an average gray level $\mu_{b.}$; and 2) other tissues/organs – low density pixels within the lungs and the surrounding regions (e.g., ribs, heart, liver, and other parts in the chest cavity). These pixels have average gray level μ_n

The segmentation algorithm consists of two steps. The first step is to select the optimum decision level to create initial labeling image that will be used in step 2. The segmentation decision level is selected through an iterative procedure. Similar to existing approaches in the literature (e.g., [10]), the new decision level for step *i + 1* is updated iteratively until there is no change using the following formula:

$$T^{i+1} = \left(\mu_b^i + \mu_n^i \right) / 2 \qquad (1)$$

The initial decision level T^o can be selected based on the CT number for pure air and CT number for pixels within the chest wall/body. In our experiments, the initial decision level has been arbitrary selected. Due to the decision level process some information may be lost due to region discontinuities so that the step 1 is not enough to create accurate segmentation for the lung regions, So the next step of our algorithm is to use Gibbs Markov Random Field (GMRF) model to extract the lung tissues from each slice.

A typical outline for statistical-based image segmentation is as follows: The observed image process G is modeled as a composite of two random processes, a high level process G^h and a low level process G^l , that is, $G = (G^h , G^l)$. Each of the three processes is a random field defined on the same lattice S. The high level process (the labeling or coloring process which computed from step 1) G^h is used to characterize the spatial clustering of pixels into regions. Fig. (1) shows Neighborhood system for Gibbs-Markov random field up to order 5 for rectangular lattice.

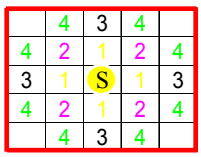

Fig. 1 Neighborhood system for Gibbs-Markov Random Field

The low level process (pixel process) $\mathbf{G}^l$ describes the statistical dependence of pixel gray level values in each region. The maximum a posteriori (MAP) segmentation involves the determination of $\mathbf{g}^h$ that maximizes $P(\mathbf{G}^h = \mathbf{g}^h \,|\mathbf{G} = \mathbf{g})$ with respect to $\mathbf{g}^h$. In order to carry out the MAP segmentation algorithm. one needs to specify the parameters in the two processes. A popular model for the high level process is the GMRF. In this paper we select the model for the low level process is Gaussian model. In order to estimate the mean and variance for each class for low level image we will use the Expectation-Maximization (EM) algorithm. In order to select the initial value of the mean for each class we compute the histogram for the low level image and select the values corresponding to the two peaks in the histogram. For binary classification (two classes), we arbitrarily select the initial estimate $\sigma^2_{C_1} = \sigma^2_{C_2} = 1$. The new mean and new variance will be computed from the following two equations.

$$\mu_{C_i}^{new} = \frac{\sum_n P(g^n / C_i) g^n}{\sum_n P(g^n / C_i)} \qquad (2)$$

$$(\sigma_{C_i}^{new})^2 = \frac{\sum_n P(g^n / C_i) \mid g^n - \mu_{C_i}^{new} \mid^2}{\sum_n P(g^n / C_i)} \qquad (3)$$

iteration stops when the new parameters are equal to the old parameters or the change is smaller than certain tolerance.

By using the iterative conditional mode (ICM) approach [11], we can classify any pixel **g** using the fact that $P(C_i/g)$ is proportional to $P(g/C_i)P(C_i/b)$; i.e.,

$$P(C_i/g) \alpha\ P(g/C_i)P(C_i/\eta_s) \qquad (4)$$

where η_s is the neighbor set to site S belonging to class C_i, $P(C_i/\eta_s)$ is computed from the following equation

$$P(C_i/\eta_s) = \frac{1}{Z} e^{-\lambda m} \qquad (5)$$

where m is the portion of η_s belonging to class C_i,
Since the algorithm compares between probabilities to find a decision, Z can be neglected. The parameter λ is the clique potential- we will set it as an arbitrary negative parameter. There exist various approaches to estimate the clique potentials in the GMRF literature (e.g., [11]) in this paper we will select λ empirically. For example $\lambda = 0$ corresponds to no dependence on the neighbors, i.e Bayes classifier. With $|\lambda|>0$, the larger the value of $|\lambda|$, the stronger is the dependence on the neighbors, and the more homogeneous results. Finally $P(g/C_i)$ is computed from the following equation

$$P(g / C_i) = \frac{1}{\sqrt{2\pi\sigma}} e^{\frac{-(g-\mu_{Ci})^2}{2\sigma_{Ci}^2}} \quad (6)$$

where μ_{C_i}, and $\sigma_{C_i}^2$ are the mean, and variance for class C_i,

2.3 DETECTING ABNORMAL TISSUES

We assume that the segmented lung volume is formed of two types of voxels: normal, which describes the healthy lung tissue, and abnormal, which describes all abnormalities in the lungs, the bronchi and bronchioles.
The first step to detect the abnormalities is to remove the normal tissues. The gray level histogram shows the distribution of the intensity of lung, which is usually a homogenous region. Lung abnormalities show in the histogram of the CT slices as bright (or homogeneous) areas with distinct gray levels from the surrounding lung tissues. Therefore, it is logical to assume that the abnormalities will correspond to the peaks (usually one) in the gray level histogram. Therefore, as a first step in isolating the abnormities, we threshold all pixels having a gray level below the gray level value of the peak of the histogram. These pixels will correspond to *normal* lung tissues.
The abnormalities, in general, appear as elliptical-shaped regions in the lungs. These elliptical shapes can be isolated by the analysis of the distribution of the gradient maxima in the neighborhood of each pixel. Ellipses and rings are patterns symmetrical relatively to their centroids. In the case of the polar co-ordinates, the expression of the intensity and spatial distribution of the most significant edges has characteristics properties of symmetry and uniformity. In the case of CT images, the gradient should show local maxima at the point on the border of the bronchi, bronchioles, and abnormal tissues.

Let I(x,y) be the image after removing the normal tissues, we consider the local polar co-ordinates (r, θ) centered at (x_o, y_o), and a neighborhood of Ω of radius r_o. the maximum of the intensity gradient within along direction θ is defined as e(θ)[12]:

$$e(\theta) = \max_{0 < r < \theta} \left(\frac{\partial I}{\partial \theta} (r, \theta) \right) \quad (7)$$

With its corresponding radius defined as r(θ). The size r_o is defined as the maximum radius of abnormality that appears in the CT scans. Fig. 2 shows a schematic representation of the definition of e (θ) , and r(θ) for a pixel (x_o, y_o) located inside an elliptical ring, shown in Fig. (2-a). By searching along direction d_θ, the gradient maximum e (θ) at distance r (θ) relatively to (x_o, y_o), shown in the gradient profile in Fig. (2-b). We note that e(θ) is the same for bronchi, bronchioles and abnormal tissues especially after we remove the normal tissues. In order to distinguish between the abnormal tissues and bronchi and bronchioles we define the following three parameters

- The value R(x, y) measures the uniformity of the radial distribution of the edges. It can be computed as

$$R(x, y) = \max(r(\theta)) - \min(r(\theta)) \quad (8)$$

- The value C(x, y) measures the connectivity that the pixel (x, y) appear in the same location in different slice
- The value P(x, y) measures the position of the pixel (x, y) right lung, or the left lung edges. P(x,y) is computed from the following equation.

$$P(x,y)=\min[abs(I(x,y)-R\_E(x_1,y_r)),abs(I(x,y_1)-L\_E(x_1,y_l))] \quad (9)$$

Where I(x,y) is the current pixel which want to classify if it is normal or abnormal tissues, $R\_E(x,y_r)$ is the position of the right edge at row x, $L\_E(x,y_r)$ is the position of the lift edge at row x
Based on the previous three parameters, we will give the following three ranks for each pixel:

- NR, this rank measures the uniformity distribution of the edges. NR is computed from the following equation

$$NR = e^{-[R(x,y)]^2} \quad (10)$$

- NC, this rank measures the connectivity that the pixel (x, y) appears in the same location in different slices. NC approaches 1 if the pixel (x, y) appears in the same location in different slice, NC becomes zero if the pixel (x, y) appears in one slice
- NP, each pixel given a rank NP reflecting its position relative to the edge of the right lung or the left lung. Since the distribution of the bronchi, and bronchioles increase in the center of the right lung, and left lung, and decrease as we move towards its edges, then NP approaches one as P(x,y) approach zero, also NP approaches zero as P (x, y) becomes large, NP will be computed from the following equation

$$NR = e^{-[P(x,y)]^2} \quad (11)$$

The three ranks are then combined to provide a list of pixels sorted according to the value of N defined as:

$$N = N_R + N_C + N_P \quad (12)$$

In our algorithm the pixel that has rank (N) greater than 2 represent the position of the most dominate abnormality elliptical ring within the image. The ranking mechanism ensures that there is no need to normalize and weight the three quantities R (x, y), C(x, y), and P(x, y). Since pixels are sorted according to each criteria independently, the final ranking does not depend on how rapidly the numerical expressions of R, C, and P increase. Since the typical size of the elliptical pattern to be identified is less than 12 pixels, it is possible to drive a precise approximation of them by considering only eight points, taken along eight principle directions, rather than considering all points of an ellipse. The eight directions are taken along horizontal, vertical, and principle diagonal axes. Edge information is derived from the image after removing the normal tissues by pre-computing the gradient along the previous 8 directions, and then computes the quantities R (x, y), C (x, y), P (x, y), NR, NC, NP, and N as illustrated in the previous section. After locating the pixels that present the center of abnormal elliptical rings, we will take it a seed to pick up all the neighbors pixels which have the same gray level from the original image.

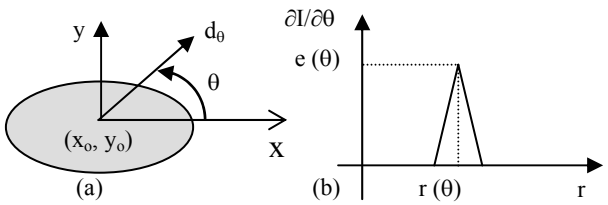

Fig. 2. **(a)** Schematic representation of the function I(x, y) for an elliptical ring. **(b)** The profile of the intensity gradient along the direction d_θ. the distance to the pixel (x_o, y_o) is denoted r. $\partial I / \partial r$ measures the intensity of the gradient.

3. RESULTS

The algorithm was evaluated on the CT scans of 50 subjects enrolled in the screening study. Ten subjects had abnormalities in their CT scans, and forty were normal. We applied the algorithm on these 50 scans. Results of the above algorithm were compared with the radiologists. Fig. 3 shows some results of isolating the lungs, bronchi and bronchioles, and abnormal tissues from a spiral CT scan of one patient enrolled in the chest screening study. We use the VTK visualization tool kit to build 3-D models for the abnormal and the entire lung regions. Fig. 4 shows an example of reconstructed lung. Table 1. Shows different shapes of abnormalities and their volume.

4. Conclusion

We have introduced a novel approach for automatic segmentation and visualization of the chest cavity from CT scans. As the resolution of the CT scans is increased, the accuracy of the reconstructed 3-D volume will increase; hence, the diagnosis of abnormal tissues Our current efforts are focused on improving the segmentation, and validating the 3-D models with respect to human experts. Long-term focus is to develop an expert system for chest cancer screening based on CT and X-ray scans.

Acknowledgement

This project is being funded by a research grant from the Jewish Hospital Foundation under project number PCF 999516

References

1. P. M. Boiselle,and C. S. White "New Technique in Thoracic Imaging" Marcel Daker Inc. 2002
2. E. A. Hoffman and G. Mclennan "Assessment of the pulmonary structure-function relationship and clinical outcomes measures: Quantitative volumetric CT of the lung," Academic Radiol., vol. 4, no. 11, pp. 758-776, 1997.
3. Robert Falk, et. al., Jewish Hospital Lung Cancer Screening & Early Detection Study, Report Dated 10/20/2000; pp. 25.
4. A. CI Henschke, et al. "Early Lung Cancer Action Project (ELCAP): Initial Findings on Repeat Screenings,". Weill Medical College, Cornell University, 2001.
5. B. D. Aberle, el al. "ACRIN PROTOCOL # 6654: Contemporary Screening for the Detection of Lung Cancer Pre-Malignancy and Malignancy," University of California - Los Angeles 2001.
6. W. A. Kalender, H. Fichte, W. Bautz, and M. Skalej, " semiautomatic evaluation procedures for quantitative CT of the lung," J. Comput. Assist. Tomogr., vol. 15, no. 2, pp. 248-255, 1991.
8. J. M. Keller, F. M. Edwards, and R. Rundle, "Automatic outlining of regions on CT scans," J. Comput. Assist. Tomogr., vol. 5, no.2, pp. 240-245, 1981.
9. D. M. Denision, M. D. L. Morgan, and A. B. Millar, "Estimation of regional gas and tissue volumes of the lung in supine man using computed tomography," Thorax, vol. 41, pp. 620-628, 1986.
10. S. Hu, E. A. Hoffman, " Automatic lung segmentation for Accurate quantitation of volumetric X-ray CT images," IEEE, Transaction on medical imaging, vol. 20, PP. 490-498, 2001.
11. Richard C. Dubes, and Anil K. Jain, " Random field models in image analysis," Journal of applied statistics, vol. 16, No. 2, pp. 131-164, 1989
12. F. Chabat, D. M. Hansel, and G. Zhong, " ERS Transformation for Detection of Bronchi on CT of the Lungs" MICCAI'99, pp. 235-244

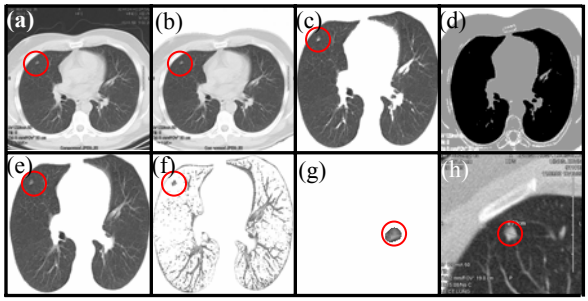

Fig. 3. : Results of segmentation, reconstruction of the lungs, and isolation of abnormal tissues for a patient enrolled in the screening program.(a): original slice from a spiral CT scan of a patient; (b) Slice after removing the background;; (c) Desired tissues; (d) High level image (Labeling Image); (e) The isolated lungs using GMRF; (f) Bronchi, bronchioles and abnormal tissues.(g) Abnormal tissues (magnified for visualization) detected by our algorithm (h) Manual detection by expert doctor

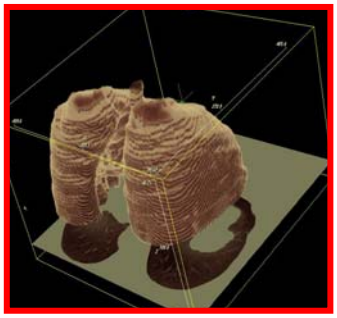

Fig. 4. 3-D Model for whole lung tissues

Abnormality					
Volume (cm3)	1.25	1.987	0.51	0.489	1.5
Cancer /No Cancer	Cancer	Cancer	Cancer	Cancer	Cancer
Abnormality					
Volume (cm3)	0.597	1.96	0.586	0.421	0.351
Cancer /No Cancer	Cancer	Cancer	Cancer	No Cancer	No Cancer

Table 1: Morphologies of 10 detected abnormalities, and the assigned diagnosis by a radiologist.